

Electrical percolation of nanoparticle-polymer composites

Guotong Wang, Chengyuan Wang*, Faling Zhang, Xiaozhu Yu

Faculty of Civil Engineering and Mechanics, Jiangsu University, No. 301 Xuefu Road, Zhenjiang, Jiangsu 212013, China



ARTICLE INFO

Keywords:

Nanoparticle-based composite
Electrical percolation
Monte Carlo simulations
Electron transport mechanism
Size and shape effects

ABSTRACT

A highly conductive and stretchable gold nanoparticle (NP)-polymer composite is achieved where some NPs are self-assembled in slender chains. It suggests an NP-chain-polymer composite with even higher electrical conductivity at much lower NP content. This study is devoted to exploring the percolation process of this new design, measuring its excellent properties and revealing the underlying physics. The Monte Carlo simulations were performed, where the van der Waals interaction and the electron tunneling between NPs are considered. It was clearly shown that the slender chains of smaller NPs lead to largely decreased percolation threshold but significantly enhanced conductivity.

1. Introduction

Flexible conductors play an indispensable role in fabricating foldable LED displays [1], conformable biosensors [2], soft energy storage devices [3,4], organic transistors [5] and smart textiles [6]. Efforts were thus invested to develop highly flexible and conductive composites [7] via the percolation of conductive nanofillers in polymers [8].

Current research is mainly focused on the composites filled with carbon nanotubes (CNTs) [9,10] and silver nanowires (AgNWs) [11,12]. Experimental techniques [11,13–15], computer simulations [11,15–19] and theoretical models [20–22] were used to study the percolation of the composites filled with the nanofillers with very large length-to-diameter aspect ratio. Major issues discussed include the effects of inter-nanofiller van der Waals (vdW) interaction, the curviness and cross-sectional size of these slender nanofillers on the percolation threshold and electrical conductivity of the composites. In addition to these slender nanofillers, metal nanoparticles (NPs) with small aspect ratio around one were also used in the composites [23–25]. A typical example is the gold NP (AuNP)-polymer composite [25] which exhibits an electrical conductivity ($\sigma_{eff} > 10^4$ S/cm), orders of magnitude higher than those with slender nanofillers [7]. A large elongation up to 484% and substantial piezo-resistive effect are also obtained [25]. These excellent properties offer a new avenue to a conformable strain/stress sensor network able to detect the stress/strain distributions on curvilinear surfaces.

In particular, some NPs [25] are found to be self-assembled via the vdW interaction to form slender chains/nanofillers. This may offer a new design with largely decreased percolation threshold but further enhanced electrical conductivity. Motivated by the properties of the

AuNP-polymer composites and the potential of this new design the present work aims to explore the distinctive percolation behavior and properties of the novel NP chain-polymer composites, reveal its electron transfer mechanisms and identify the key factors controlling the percolation process. The emphasis of the present study was placed on the key factors that determine the percolation threshold and the conductivity of the composite at different stages. These factors include the conductivity, shape and size of NPs, and the electron tunneling energy barrier of the matrix, which were not discussed in detail in previous studies. The present work thus has brought in new insights into the percolation behavior and the underlying physics for the conductive nanocomposite.

2. Methodology

2.1. Construction of the NP-matrix system

Here the goal was to construct a representative volume element (RVE) of the NP-based composites. Two different cases were considered, i.e., (1) NPs are chained to form slender nanofillers and (2) some NPs are self-assembled in chains while others are distributed randomly in the matrix. Attention was mainly focused on the first case. The second one was considered to reveal the shape effect of the nanofillers. To simplify the analysis, the NPs are treated as spheres of diameter D .

First, a hollow circular cylinder was created in an empty cubic. Its geometric center (x, y, z) was generated randomly in the cubic. To reproduce the structure of the composites synthesized by the layer by layer technique [25], the central line of the cylinder stays in a plane

* Corresponding author.

E-mail address: cywang@ujs.edu.cn (C. Wang).

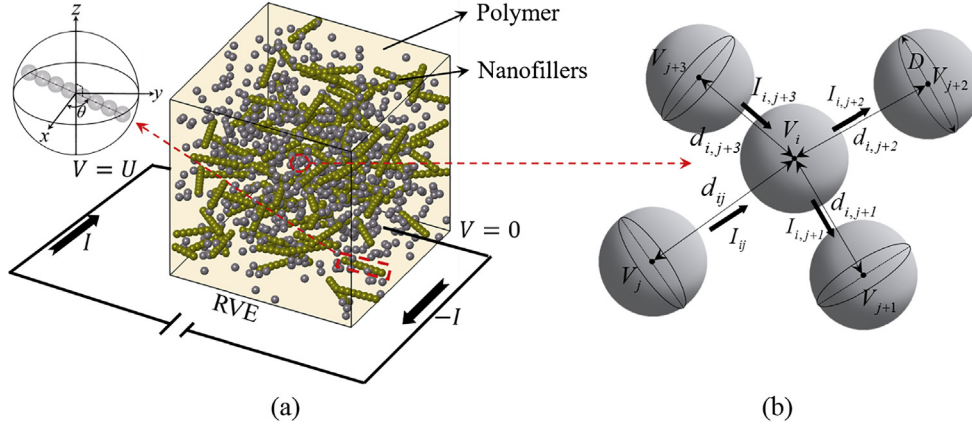


Fig. 1. Schematic of (a) a resistor model with some NPs chained in the slender nanofillers and (b) the electrical current between the i -th NP and its neighbors.

parallel with the XY plane. The orientation of the central line can then be specified by the angle θ between the central line and the X axis (Fig. 1). Here, θ is generated randomly between 0° and 360° . The diameter of the cylinder is equal to D and its length L is given by $L = ND + (N-1)d_{eq}$ where N is the number of NPs in the cylinder and d_{eq} is the distance between neighboring NPs. Here, $d_{eq} = 0.273$ nm is the equilibrium distance between NPs due to the vdW interaction. The value was obtained in our molecular dynamics simulations at $D = 5$ nm. Its dependence on the diameter and material of NPs is neglected. In this study, 12 NPs (i.e., $N = 12$) were placed in the cylinder with their geometric centers on the central line. Slender nanofiller were then achieved with diameter D , length L and aspect ratio $\frac{L}{D} = 12 + \frac{3}{D}$, which varies from 12.1 to 12.6 when D is in the range of [5 nm, 30 nm] and is close to the experimental observation [25]. Increasing the number of nanofillers we finally achieved a RVE with slender nanofillers and the desirable NP volume fraction (VF). Herein, the distance between the NP centers in different cylinders was kept larger than D to avoid the penetration of the nanofillers.

In addition, to distribute NPs outside the chains we randomly generated a point (x, y, z) and placed an NP at the point when its distance to the centers of the chained NPs was greater than D . Then we increase the number of NPs by repeating the procedure until the desired VF was achieved. In doing this, we assumed that the randomly distributed NPs are the ‘soft-core’ capped spheres and thus allowed to penetrate the adjacent ones. This will lead to some errors in predicting the percolation properties but their trend to change with the number of the chained NPs should be correct.

In generating the coordinates (x, y, z) , we adopted the multiplicative congruential (MC) generator, the most common computer technique for producing random sequences. In the simulation, the MC generator can generate three random numbers $x, y,$ and z ranging from 0 to 1, giving the coordinates of a randomly selected point [26,27].

2.2. Model of NP electrical contact

In Section 2.1 a RVE of the NP-based composite was achieved in Fig. 1a. Two electrodes were attached and an electrical voltage U was then applied to the RVE. When the NP content becomes sufficiently large the adjacent NPs will be in touch electrically (Fig. 1b). It is thus essential to define the conditions of NP electrical contacts.

Herein, NPs cannot be in physical contact due to the vdW interaction between them. Specifically, there exists an equilibrium distance d_{eq} between NPs associated with the minimum cohesive energy and zero vdW interaction. The distance d_{ij} between the i -th NP and j -th NP ($i, j = 1, 2, 3, \dots$) is defined in Fig. 2 as the distance between their centers L_{ij} minus the diameter D . Two NPs were considered in electrical contact with zero contact electrical resistance, i.e., $R_{ij}^0 = 0$, when $d_{ij} \leq d_{eq}$ (Fig. 2a). When the NPs become wider apart with $d_{ij} > d_{eq}$, they are

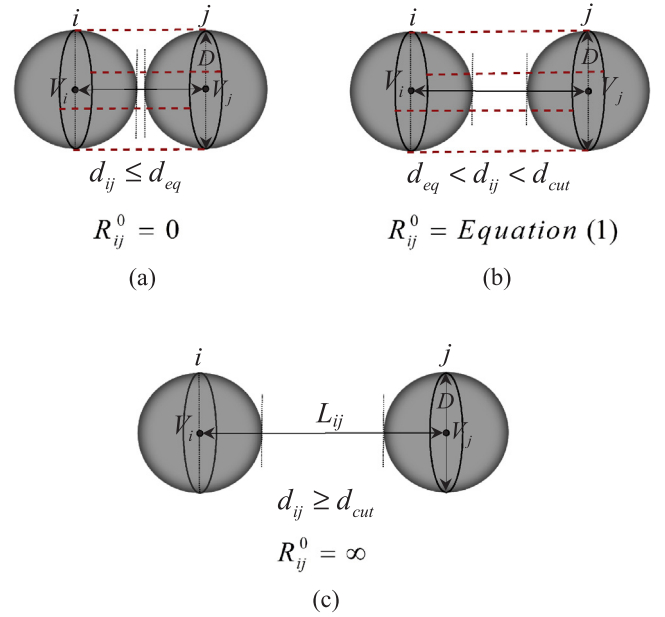


Fig. 2. Electrical connections between two NPs, i.e., (a) conductive contact, (b) electron tunneling junction and (c) no electrical current.

still in electric contact due to electron tunneling between them. In this case, the contact electrical resistance R_{ij}^0 is given by (Fig. 2b)

$$R_{ij}^0 = \frac{V_{ij}}{AJ} = \frac{h^2 d_{ij}}{Ae^2 \sqrt{2m\lambda}} \exp\left(\frac{4\pi d_{ij}}{h} \sqrt{2m\lambda}\right) \quad (1)$$

where J is tunneling current density, V_{ij} is the electrical potential difference of the NPs, e is the single electron charge, m is the mass of electron, h is Planck's constant, λ is the height of the energy barrier, and A is the cross-sectional area of the tunnel, which is assumed to be the same as the cross-sectional area of NPs. When the distance d_{ij} further increases, and becomes greater than a cutoff distance d_{cut} , R_{ij}^0 is considered as infinitely large and the two NPs are disconnected. In this work, d_{cut} is chosen as 1.5 nm as our study showed that further increasing the value does not significantly change the results. Herein, it is worth mentioning that d_{cut} may change with the size of the NPs. However, this radius-dependence is not considered for d_{cut} in previous studies [11,17,19]. In particular, good agreement has been achieved between the simplified model and experiments [11], which seems to suggest that such an effect of NP radius can be safely neglected. Thus, following the existing studies the simplified model was employed in the present study where d_{cut} is assumed to be independent of NP size. The total electrical resistance ($R_{ij} = R_{ij}^0 + R_{NP}$) between the i -th NP and the j -

th NP was calculated as (1) $R_{ij} = R_{NP}$ at $d_{ij} \leq d_{eq}$; (2) $R_{ij} = R_{ij}^0 + R_{NP}$ (R_{ij}^0 is given by Eq. (1) at $d_{eq} < d_{ij} < d_{cut}$ and (3) $R_{ij} = \infty$ at $d_{ij} \geq d_{cut}$. Here $R_{NP} = \frac{2}{\pi D} \rho_{NP}$ is the equivalent electrical resistance of individual NPs and ρ_{NP} is the electrical resistivity of the NPs.

2.3. Electrical resistor model

In the RVE (Fig. 1a), for the i -th and j -th NPs ($i, j = 1, 2, 3, \dots, N$ and $i \neq j$) the electrical potentials are V_i and V_j , respectively and the conductance between them is $a_{ij} = 1/R_{ij}$. Based on the Ohm's law, the electrical current I_{ij} between them can be calculated by $I_{ij} = a_{ij}(V_j - V_i)$. In addition, the Kirchhoff's current law states that the summation of the electrical currents flowing into and outside the i -th NP must be zero (Fig. 1b), i.e., $\sum_{j=1}^N I_{ij} = 0$ or

$$a_{ii}(V' - V_i) + \sum_{j \neq i}^N a_{ij}(V_j - V_i) = 0 \quad (2)$$

As shown in Fig. 1, $V' = U$ represents the potential of one electrode. The other electrode is grounded with its potential equal to zero. Eq. (2) can be rewritten as

$$\left(a_{ii} + \sum_{j=1}^N a_{ij} \right) V_i - \sum_{j=1}^N a_{ij} V_j = a_{ii} V' \quad (3)$$

Subsequently, an iterative equation solver (i.e., the incomplete Cholesky conjugate gradient method) was employed to solve the above large-scale linear equations. The electrical potentials of the NPs can be obtained and those of the NPs in electrical contact with the electrodes were used to estimate the total electrical current I through the RVE. The effective electrical conductivity of the RVE is evaluated by $\sigma_{eff} = \frac{I L}{U S}$, where L is the distance between the two electrodes and S is their cross-sectional area (Fig. 1a).

The method demonstrated above was used to plot the percolation curve for AuNP-polymer composite where α (α is defined as the number of the AuNPs chained (in the cylindrical nanofillers)-to-the total number of AuNPs ratio) varies from 0 to 0.4 and 1, and the radius of AuNP is fixed at 13 nm. The maximum conductivity obtained (10^4 S/cm) is found to be in good agreement with the experiment [25] where the radius of AuNPs is also 13 nm. In addition, with α greater than 0.4 the percolation threshold obtained is close to 15.4% obtained in the experiment [25] where some of the AuNPs were chained to form slender nanofillers (The value of α however is not specified in [25]). The comparison thus showed the relevance of the present simulation method to the percolation behavior of the NP-based composites. More details of the analyses will be shown later in Section 3.2.

3. Results and discussions

3.1. Physical mechanisms of electrical percolation

An empirical power law is achieved, i.e., $\sigma_{eff} = \sigma_0(VF - VF_{cr})^t$ for electrical percolation of metal particle-based composites [14–16]. Here σ_0 and σ_{eff} are the electrical conductivity of the particles and the composite, respectively, exponent t is a constant and VF_{cr} represents the percolation threshold. In this study, σ_{eff} was calculated for different VFs and the percolation curves were obtained by fitting the power law to the simulations in Fig. 3a for the composites with 100% of the AuNPs (diameter 13 nm) chained in slender nanofillers ($\alpha = 1$) Herein, three different polymer matrixes were considered with $\lambda = 0.5$ eV, 1 eV and 2 eV, respectively, as it is reported in [15,21] that λ of epoxy and PDMS falls in the range of [0.5 eV, 2.5 eV]. Fig. 3b was obtained for those comprising of the matrix with $\lambda = 1$ eV, but three different NPs (diameter 13 nm) whose $\rho_{NP} = 1.7 \mu\Omega\cdot\text{cm}$ (CuNP), $2.4 \mu\Omega\cdot\text{cm}$ (AuNP) and

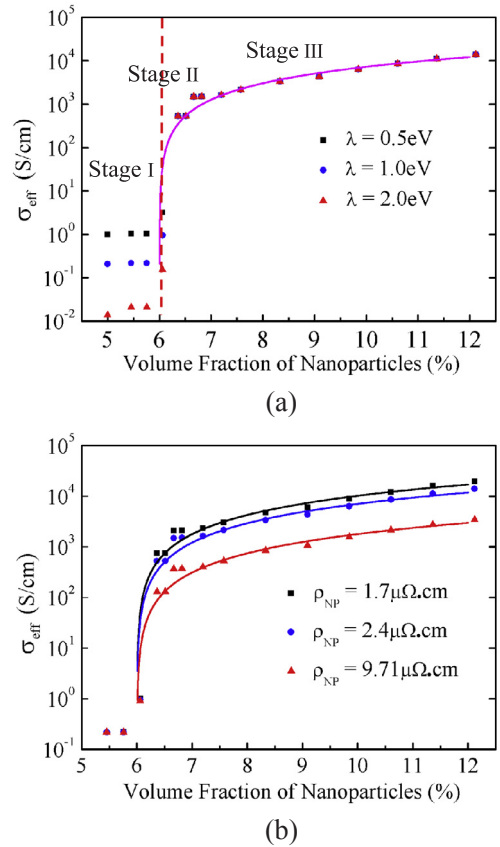


Fig. 3. (a) The effect of tunneling energy barrier λ on the conductivity. Herein, $D = 13$ nm, $\alpha = 1$, $\rho_{NP} = 2.4 \mu\Omega\cdot\text{cm}$. (b) The effect of NP resistivity ρ_{NP} on the conductivity. $D = 13$ nm, $\alpha = 1$, $\lambda = 1.0$ eV are considered.

$9.71 \mu\Omega\cdot\text{cm}$ (FeNP), respectively.

As expected, similar percolation behavior is observed in Fig. 3 for all composites considered with nearly the same percolation threshold $VF_{cr} = 6\%$ and a constant exponent $t = 1.26$ in the power law. Thus, the position (i.e., VF_{cr}) and the profile (i.e., t) of the percolation curves should be independent of the material properties of the components. At $VF < VF_{cr}$ (stage I), σ_{eff} grows gradually with rising VF and is in the order of $10^{-2} \sim 10^0$ S/cm. When VF reaches VF_{cr} (stage II) a sudden growth occurs with σ_{eff} climbing up from $10^{-2} \sim 10^0$ S/cm to 10^3 S/cm. At $VF > VF_{cr}$ (stage III) σ_{eff} again increases progressively with rising VF . It reaches 10^4 S/cm at $VF = 11.5\%$ for the AuNP-based composite.

As noted in Fig. 3a, σ_{eff} increases significantly with the decreasing energy barrier λ but becomes less sensitive to the variation of VF at stage I. From Eq. (1) it is seen that the contact electrical resistance (R_{ij}^0) increases rapidly with $\sqrt{\lambda}$ when the current is achieved via the electron tunneling. Thus, rising σ_{eff} with decreasing λ observed at stage I should be a result of the lower contact resistance (R_{ij}^0) given by Eq. (1). This indicates that, at stage I an integrate electrical circuit is established in the RVE where the conductivity is controlled by the electron tunneling between NPs. In contrast, the conductivity and its VF -dependence at stage III remain nearly unchanged for different λ (Fig. 3a), showing that the electron tunneling has almost no influence on stage III.

In addition, we see from Fig. 3b that raising resistivity ρ_{NP} of the NPs by a factor of 2 to 4 can substantially decrease σ_{eff} at stage III. For example, at $VF = 12\%$ σ_{eff} declines by 2 and 8 times, respectively, once CuNPs are replaced by AuNPs and FeNPs. Herein, the high σ_{eff} and the strong effect of ρ_{NP} at stage III suggest that an integrate electrical circuit has been constructed, where the distance between adjacent NPs is smaller than d_{eq} and thus, the constituent NPs are in conductive contact with zero contact electrical resistance (Section 2.2). On the contrary, the variation of ρ_{NP} does not affect the conductivity at stage I controlled

by the electron tunneling. The results in Fig. 3 thus show the switch of the electron transport mechanism from electron tunneling to conductive contacts when VF reaches the percolation threshold.

It was reported in [25] that at stage III σ_{eff} of the AuNP-polymer composite changes significantly with applied strain, which makes the composite promising for piezo-resistive strain sensors. Based on the present study, such a piezo-resistive effect may also be achieved at stage I controlled by the electron tunneling between NPs and thus, very sensitive to the variation of the NP distance (see Eq. (1)) induced by strain. Also, Fig. 3a shows that a higher energy barrier λ leads to higher sensitivity of σ_{eff} to the variation of VF or the distance between NPs. Also the possible strain-dependence of λ may enable one to further enhance the piezo-resistivity via the strain-induced growth of λ . It is thus expected that selecting a proper polymer matrix with relatively large λ that rises with increasing strain may lead to greatly enhanced piezo-resistivity relative to that of stage I. In addition, the lower VF of NPs at stage I may also results in a low stiffness but high stretch-ability as compared with stage III.

3.2. Size and shape effects of nanofillers

In this section, we first examined the size effect of the NPs. The AuNP-based composite with $a = 1$ was used as an example. The obtained percolation curves were plotted in Fig. 4 for AuNP diameter 20 nm, 13 nm and 5 nm, respectively. The associated percolation threshold VF_{cr} shown in Fig. 4 was found to decrease from around 6.1% to 6% and 5.5%. In this process, the power exponent t also declined from 1.3 to 1.28 and 1.22 due to the decreasing size of AuNPs, i.e., the rate of change in σ_{eff} with VF became smaller. Despite of the decreasing t , smaller AuNPs generally lead to a higher electrical conductivity at stage III (Fig. 4). For example, at $VF = 11\%$, the electrical conductivity can be raised from 8.37×10^3 S/cm, to 9.12×10^3 S/cm and 1.24×10^4 S/cm by a factor of 1.09 and 1.48, respectively, when the AuNP diameter decreases from 20 nm to 13 nm and 5 nm. It follows that smaller NPs will lead to lower VF_{cr} but higher σ_{eff} at stage III. In particular, such a size effect is found to be more pronounced for smaller NPs. The possible physical mechanism is that, for a given VF larger NPs will lead to increased average distance d_{ij} between NPs [28].

It is noted in Figs. 3 and 4 that the maximum σ_{eff} obtained for the composites filled with 13 nm AuNPs is around 10^4 S/cm in agreement with the experiment [25] (Fig. 5). Nevertheless, the percolation threshold 6% shown in Figs. 3 and 4 is much smaller than 15.4% obtained in the experiment [25]. The discrepancy may arise from the fact that the slender nanofillers ($a = 1$) were considered in Figs. 3 and 4, while some NPs are randomly distributed in [25]. To examine the shape effect of nanofillers, we studied the AuNP-based composites in three cases, i.e., (1) All AuNPs are randomly distributed without chained AuNPs ($\alpha = 0$); (2) 40% of the AuNPs are chained and 60% of them are

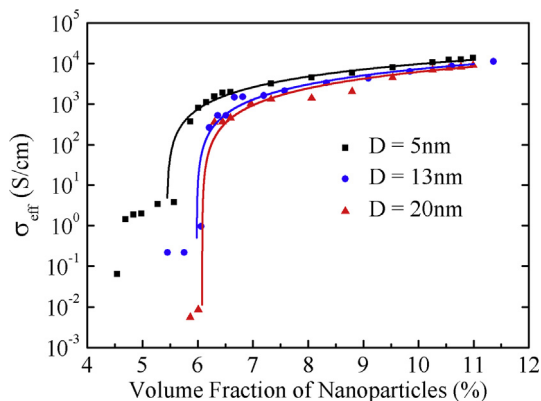


Fig. 4. Size effect of NPs on the percolation of the NP chain-based composites. Herein, $\alpha = 1, \rho_{NP} = 2.4 \mu\Omega \cdot \text{cm}, \lambda = 1.0$ eV.

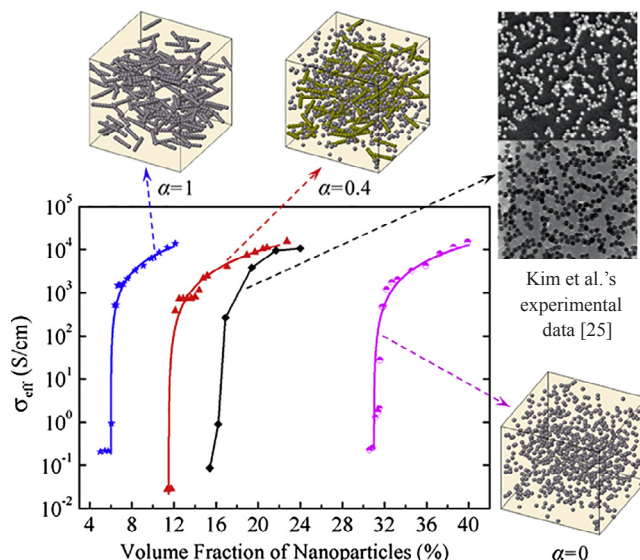


Fig. 5. The effect of the parameter α on the conductivity of nanocomposite. Herein, $D = 13$ nm, $\lambda = 1.0$ eV, $\rho_{NP} = 2.4 \mu\Omega \cdot \text{cm}$.

randomly distributed ($\alpha = 0.4$) and (3) all AuNPs are chained to form the slender nanofillers ($\alpha = 1$). The percolation curves and the corresponding RVEs were shown in Fig. 5 in comparison with the ones obtained in the experiment [25].

It is seen that when slenderer nanofillers are found with α growing from 0 to 0.4 and to 1, the percolation curve moves to the left with VF_{cr} decreasing from around 31% to 11.5% and 6%. These results manifest the shape effect of the nanofillers on the percolation threshold. Specifically, considering the proper α we would be able to achieve the results close to the experimental data [25] (Fig. 5). The figure thus demonstrates the relevance of the Monte Carlo simulations to the percolation of the NP-based composites. In addition, the curve fitting also shows that the exponent t of the percolation law changes from 1.45 to 1.55 and 1.27 when α rises from 0 to 0.4 and 1. From the above analyses it follows that, the percolation threshold and power exponent are determined solely by the geometric characteristics of nanofillers but independent of the material properties of constituent NPs and matrix. The results indicated that constructing long NP chains (e.g., aspect ratio 50) of small AuNPs (e.g., diameter 5 nm) one can expect to achieve a NP chain-based composite with, e.g., $VF_{cr} = 1\%$ or lower, and the conductivity approaching 10^5 S/cm of pure gold.

4. Conclusions

The percolation process was studied for highly conductive NP chain-polymer composites based on the Monte Carlo simulations and the theory of electrical circuit. It is found that the percolation threshold signifies the switch of the electron transport mechanism from the electron tunneling to the conductive contact of NPs. In particular, the conductivity at stage I is mainly determined by the tunneling energy barrier of the matrix while the one at stage III is primarily controlled by the electrical resistivity of NPs. Substantial effect of piezo-resistivity is thus expected at stage I, which can be further enhanced by selecting a polymer matrix with large energy barrier that increases with rising tensile strain.

In contrast to these, the percolation threshold and the power exponent are independent of the material properties of the NPs and matrix but fully decided by the size and shape of the nanofillers. Decreasing NP size and, especially, chaining NPs to form slender nanofillers can efficiently reduce the percolation threshold and further improve the overall conductivity of the composite. The NP chain-polymer composites are promising for the material with very low NP content but the

conductivity approaching that of pure metal.

Acknowledgement

Financial support from the General Program of Jiangsu Natural Science Foundation of China (Grant No. SBK2015020787), Youth Fund of Jiangsu Natural Science Foundation of China (BK20140523), Start-up Research Fund for Advanced Talent of Jiangsu University (15JDG042) is greatly appreciated.

References

- [1] T. Sekitani, H. Nakajima, H. Maeda, T. Fukushima, T. Aida, K. Hata, T. Someya, *Nat. Mater.* 8 (2009) 494–499.
- [2] X. Huang, W.H. Yeo, Y.H. Liu, J.A. Rogers, *Biointerphases* 7 (2012) 52.
- [3] X.F. Wang, X.H. Lu, B. Liu, D. Chen, Y.X. Tong, G.Z. Shen, *Adv. Mater.* 26 (2014) 4763–4782.
- [4] X.F. Wang, K. Jiang, G.Z. Shen, *Mater. Today* 18 (2015) 265–272.
- [5] T. Sekitani, T. Yokota, U. Zschieschang, H. Klauk, S.F. Bauer, K. Takeuchi, M. Takamiya, T. Sakurai, T. Someya, *Science* 326 (2009) 1516–1519.
- [6] M. Stoppa, A. Chiolerio, *Sensors* 14 (2014) 11957–11992.
- [7] S.S. Yao, Y. Zhu, *Adv. Mater.* 27 (2015) 1480–1511.
- [8] J. Hoshen, R. Kopelman, *Phys. Rev. B* 14 (1976) 3438–3445.
- [9] C.J. Yu, C. Masarapu, J.P. Rong, B.Q. Wei, H.Q. Jiang, *Adv. Mater.* 21 (2009) 4793–4797.
- [10] S.M. Shang, W. Zeng, X.M. Tao, *J. Mater. Chem.* 21 (2011) 7274–7280.
- [11] M. Amjadi, A. Pichitpajongkit, S.J. Lee, S. Ryu, I. Park, *ACS Nano* 8 (2014) 5154–5163.
- [12] C.H. Liu, X. Yu, *Nanoscale Res. Lett.* 6 (2011) 75.
- [13] R. Ramasubramaniam, J. Chen, H.Y. Liu, *Appl. Phys. Lett.* 83 (2003) 2928–2930.
- [14] D.S. McLachlan, C. Chiteme, C. Park, K.E. Wise, S.E. Lowther, P.T. Lillehei, E.J. Siochi, J.S. Harrison, *J. Polym. Sci. Part B: Polym. Phys.* 22 (2005) 3273–3287.
- [15] N. Hu, Z. Masuda, C. Yan, G. Yamamoto, H. Fukunaga, T. Hashida, *Nanotechnology* 19 (2008) 215701.
- [16] H.M. Ma, X.L. Gao, *Polymer* 49 (2008) 4230–4238.
- [17] N. Hu, Y. Karube, C. Yan, Z. Masuda, H. Fukunaga, *Acta Mater.* 56 (2008) 2929–2936.
- [18] T. Zhang, Y.B. Yi, *J. Appl. Phys.* 103 (2008) 014910.
- [19] W.B. Lu, T.W. Chou, E.T. Thostenson, *Appl. Phys. Lett.* 96 (2010) 223106.
- [20] G.D. Seidel, D.C. Lagoudas, *J. Compos. Mater.* 43 (2009) 917–941.
- [21] T. Takeda, Y. Shindo, K. Yu, F. Narita, *Polymer* 52 (2011) 3852–3856.
- [22] C. Feng, L. Jiang, *Compos. Part A Appl. Sci. Manuf.* 47 (2013) 143–149.
- [23] B.Y. Ahn, E.B. Duoss, M.J. Motala, X.Y. Guo, S.I. Park, Y.J. Xiong, J.S. Yoon, R.G. Nuzzo, A.J. Rogers, J.A. Lewis, *Science* 323 (2009) 1590–1593.
- [24] D.C. Hyun, M. Park, C.J. Park, B. Kim, Y. Xia, J.H. Hur, J.M. Kim, J.J. Park, U. Jeong, *Adv. Mater.* 23 (2011) 2946–2950.
- [25] Y. Kim, J. Zhu, B. Yeom, M.D. Prima, X. Su, J.G. Kim, S.J. Yoo, C. Uher, N.A. Kotov, *Nature* 500 (2013) 59–64.
- [26] S.L. Anderson, *SIAM Rev.* 32 (1990) 221–251.
- [27] S.K. Park, K.W. Miller, *Commun. ACM* 31 (1988) 1192–1201.
- [28] Y. Wang, C.Y. Wang, G.T. Wang, R.J. Wang, *Comput. Mater. Sci.* 134 (2017) 58–66.